Journal of Power Sources 196 (2011) 747–753

Contents lists available at ScienceDirect

Journal of Power Sources

journal homepage: www.elsevier.com/locate/jpowsour

Hydrogen purification for fuel cell using $CuO/CeO_2–Al_2O_3$ catalyst

Cristhiane Guimarães Maciel[a,*], Luciene Paula Roberto Profeti[b,2], Elisabete Moreira Assaf[b,2], José Mansur Assaf[a,1]

[a] Universidade Federal de São Carlos, Departamento de Engenharia Química, Via Washington Luiz, Km 235, CEP: 13565-905, São Carlos, SP, Brazil
[b] Universidade de São Paulo, Departamento de Físico-Química, Avenida Trabalhador São Carlense 400, CEP: 13560-970, São Carlos, SP, Brazil

ARTICLE INFO

Article history:
Received 2 June 2010
Received in revised form 24 July 2010
Accepted 26 July 2010
Available online 3 August 2010

Keywords:
Hydrogen purification
Copper
Ceria support
Alumina support
Preferential CO oxidation

ABSTRACT

CuO/CeO_2, CuO/Al_2O_3 and $CuO/CeO_2–Al_2O_3$ catalysts, with CuO loading varying from 1 to 5 wt.%, were prepared by the citrate method and applied to the preferential oxidation of carbon monoxide in a reaction medium containing large amounts of hydrogen (PROX-CO). The compounds were characterized *ex situ* by X-ray diffraction, specific surface area measurements, temperature-programmed reduction and temperature-programmed reduction of oxidized surfaces; XANES-PROX *in situ* experiments were also carried out to study the copper oxidation state under PROX-CO conditions. These analyses showed that in the reaction medium the Cu^0 is present as dispersed particles. On the ceria, these metallic particles are smaller and more finely dispersed, resulting in a stronger metal–support interaction than in CuO/Al_2O_3 or $CuO/CeO_2–Al_2O_3$ catalysts, providing higher PROX-CO activity and better selectivity in the conversion of CO to CO_2 despite the greater BET area presented by samples supported on alumina. It is also shown that the lower CuO content, the higher metal dispersion and consequently the catalytic activity. The redox properties of the ceria support also contributed to catalytic performance.

1. Introduction

Fuel cells have attracted great interest in the last few years as one of the most promising environmentally friendly systems for energy generation. The polymer electrolyte membrane fuel cell (PEMFC) has been the center of attention among research groups around the world for its particular use in small-scale and automotive applications [1–5].

The hydrogen utilized as fuel in these cells is mainly generated by steam reforming of hydrocarbons or alcohols, followed by the two-stage water gas shift reaction (WGSR). Typical effluents coming from such processes contain about 45–75 vol.% H_2, 15–25 vol.% CO_2, 1.3 vol.% CH_4, 10 vol.% H_2O and 0.5–2 vol.% of CO. Since CO at this concentration is poisonous to the Pt electrode in the PEMFC, purification of the effluent is needed to reduce CO concentration to under 100–10 ppm, which can be tolerated by modern Pt-alloy electrocatalysts [1,6–7]. The CO purification methods available include the use of Pd or Pt-alloy membranes, methanation or preferential oxidation of CO (PROX-CO). Many researchers believe that PROX-CO is one of the most promising methods for CO removing [1,4].

The PROX-CO reaction involves the oxidation of CO to CO_2 (Eq. (1)) without simultaneously oxidizing H_2 to H_2O (Eq. (2)).

$$CO + ½O_2 \rightarrow CO_2 \quad (1)$$

$$H_2 + ½O_2 \rightarrow H_2O \quad (2)$$

Reaction (1) is more exothermic than reaction (2) ($\Delta H^\circ = -280$ and $-240\,kJ\,mol^{-1}$, respectively) [1,8]. Reaction (1) should be avoided by the formation of water reduces from the amount of hydrogen available to operate the fuel cell and thus the energy conversion efficiency of the system can be reduced [6].

PROX-CO has been extensively investigated and there are two ideal temperatures for the reactor: either the PEMFC operating temperature itself (80–100 °C) or the temperature of the reformer unit (250–300 °C). Another crucial requirement for the PROX reactor is a high rate of CO oxidation [1,6].

Most catalysts proposed for PROX-CO reaction are alumina-supported platinum group metals and gold based catalysts, especially small particles of Au (<5 nm). However, the use of noble metals is limited due to their high activity for H_2 oxidation above 100 °C and their high cost and limited availability [1,7–8]. A PROX-CO model reactor with a noble metal catalyst has, however, demonstrated that it is very hard to reduce CO to a few tens of ppm in a single-stage reactor, because of the extremely poor selectivity of the catalyst at very low CO concentrations. Hence, a staged reactor is used for the CO clean-up with Pt catalysts. On the other hand, the use of a different reactor is not necessary for ceria-supported

* Corresponding author. Tel.: +55 16 8165 6998; fax: +55 16 3351 8266.
E-mail address: crisqui@gmail.com (C.G. Maciel).
[1] Fax: +55 16 3351 8266.
[2] Fax: +55 16 3373 9903.

0378-7753/$ – see front matter © 2010 Elsevier B.V. All rights reserved.
doi:10.1016/j.jpowsour.2010.07.061

copper catalysts, since they have excellent selectivity and high catalytic activity comparable with or better than that of noble metal catalysts [9].

Catalysts supported on ceria have a wide range of applications, including three-way catalysis, removal of SOx–NOx and various oxidation and hydrogenation reactions. Cerium dioxide can perform the functions of stabilizing the metal dispersion, storing and releasing oxygen and improving CO oxidation and NOx reduction [10]. Ceria has the capability of promoting oxidation reactions, as it generates oxygen vacancies that form interfacial active centers. As a consequence, metal–support interaction can be stabilized, explaining the high catalytic performance in specific reactions. The role of ceria is not only related to its oxygen storage capacity, but also to its ability to improve the dispersion of the supported metals [11]. The redox and catalytic properties of CeO_2 and related materials are associated with the crystal size and structural defects such as oxygen vacancies [1].

Recently, CuO/CeO_2 catalysts have been found to be effective for low-temperature CO oxidation, their activities being comparable even to those of precious metals. This high activity is attributed to the rapid reversibility of Cu^{2+}/Cu^{+} redox couples and also to a good dispersal of copper species over the ceria [10,12–13]. The high activity of surface copper species induced by their interaction with CeO_2 was identified by Manzoli et al. as the determining factor for the good activity of those solids [14]. Zhou et al., by observing the reduction-oxidation activity of copper Cu^{2+}/Cu^{+} (Cu^0) and ceria Ce^{4+}/Ce^{3+}, concluded that the redox properties of ceria can have a key role in governing the catalytic behavior [12].

Gómez-Córtes et al. reported that the CO oxidation activity of CuO/CeO_2 catalysts is associated to the concentration and especially the state of dispersion of Cu species in the catalyst. Variations in the methods of preparation might lead to a better dispersion of copper species. Another strategy for improving the dispersion of the copper phase is to modify the surface area of the support [1].

In the present study, catalysts with CuO contents of 5, 2.5 and 1 wt.% supported on CeO_2, Al_2O_3 and CeO_2–Al_2O_3 were prepared, characterized and tested for catalysis of preferential CO oxidation. The aim of this work was to investigate the influence of CuO content and the support effect on the catalysts, tested on the PROX-CO reaction in the presence of a great excess of H_2.

2. Experimental

2.1. Preparation of catalysts

The catalyst precursors were synthesized by the citrate method from solutions of $Cu(NO_3)_2{\cdot}3H_2O$, $Ce(NO_3)_3{\cdot}6H_2O$ and $Al(NO_3)_3{\cdot}9H_2O$. Nine catalysts were prepared: (a) xCuO/CeO_2, (b) xCuO/Al_2O_3 and (c) xCuO/CeO_2–Al_2O_3, where x is 1, 2.5 or 5 wt.%. The CeO_2:Al_2O_3 molar ratio was held in 1:5. A solution of citric acid was added to a solution of the mixed metal nitrates at 60 °C, with stirring. After a few minutes, ethylene glycol was also added. The resulting solution was evaporated at 110 °C for 48 h and a spongy material was formed. The product was ground and dried at 60 °C for 24 h. Finally, the solids were calcined in oxidant atmosphere at 500 °C for 5 h, after being heated at 1 °C min^{-1}.

2.2. Characterization of catalysts

X-ray powder diffraction (XRD) was carried out in a Rigaku Multiflex diffractometer with CuKα radiation. The X-ray spectra were identified by comparison with the JCPDS patterns. The surface area was measured by the N_2-adsorption - BET method in a Quantachrome Nova 1200 surface analyzer. Information on the reducibility of the bulk oxide species was obtained by temperature-programmed reduction (H_2-TPR) and that of the oxidized surface species by s-TPR in a Micromeritics Pulse Chemisorb 2705, using a heating rate of 10 °C min^{-1} from room temperature up to 900 °C. The reducing gas was a 5% H_2/N_2 mixture, flowing at 30 cm^3 min^{-1}. The s-TPR was used to calculate the copper dispersion (D_{Cu}), metal surface area (MSA) and average copper particle size (AV), as described by Gervasini et al. [15]. The experiment involved the following steps: reduction with 5% H_2/N_2 mixture, followed by re-oxidation of the surface Cu^0 under mild conditions with N_2O, at 60 °C; finally reduction with 5% H_2/N_2 mixture, heating at 10 °C min^{-1} from room temperature to 600 °C. The total amount of reduced Cu was determined by integration of the reduction peaks of the first step. From the amount of H_2 consumed in the second reduction, the total surface Cu was determined. Both Cu surface area and Cu particle size were calculated by assuming a surface Cu concentration of 1.47×10^{19} atoms m^{-2}. The Cu dispersion (%) was calculated by the formula: $D_{Cu} = 100 \times Cu_{surface}/Cu_{total}$. The xCuO/CeO_2 catalysts were chosen as representative samples to perform this analysis.

In situ energy-dispersive H_2-TPR/XANES measurements at the Cu K-edge (8979 eV) were performed in the transmission mode at the D06-DXAS synchrotron beam line at LNLS, Brazil, using a pressed pellet of about 100 mg of the catalyst. The pellet was mounted in a stainless steel holder placed in the center of a temperature-controlled flow reactor cell, into which a reactant gas or an inert gas was introduced. The reactor was a quartz tube closed at each end with aluminum flanges sealed by Kapton windows, heated in a compact furnace with halogen lamps as heater elements. The XANES spectra were recorded as the reactant gas (H_2/N_2, 5%) flowed through the samples (30 cm^3 min^{-1}) and the temperature was raised at 10 °C min^{-1} up to 300 °C. Prior to the experiments, the reactor was purged with He for more than 30 min at a flow rate of 30 cm^3 min^{-1}. The flow of each gas was regulated by a separate mass flow controller. The beam line was equipped with a Si (1 1 1) polychromator crystal operating in Bragg mode, to select the desired range of X-ray energy (8860–9100 eV), and the beam was focused on the sample. A pixel CCD solid-state detector was used as recorder and the spectra were collected with 15 ms exposure time and 50 scans for each edge. A spectrum was collected from a Cu foil for energy calibration.

2.3. Catalytic activity measurements

Catalytic activities in the PROX-CO were measured at atmospheric pressure, with a feed of 4%CO, 2%O_2, 50%H_2 and N_2 balance. The tests were performed while decreasing the temperature from 300 to 100 °C in steps of 50 °C. The samples were reduced *in situ* with pure H_2 at 300 °C, flowing at 30 cm^3 min^{-1} for 2 h, before their activity was measured. The reactions products were analyzed with an in-line chromatograph (VARIAN GC 3800) with two thermal conductivity detectors and packed columns of Porapak N and 13X molecular sieve.

The conversions of CO (XCO) and of O_2 (XO_2), and the selectivity for CO oxidation (SCO) in hydrogen excess, were calculated as follows:

$$X_{(CO)}\,\% = \frac{[CO]_{in} - [CO]_{out}}{[CO]_{in}} \times 100$$

$$X_{(O_2)}\,\% = \frac{[O_2]_{in} - [O_2]_{out}}{[O_2]_{in}} \times 100$$

$$S(CO)\,\% = \frac{0.5([CO]_{in} - [CO]_{out})}{[O_2]_{in} - [O_2]_{out}} \times 100$$

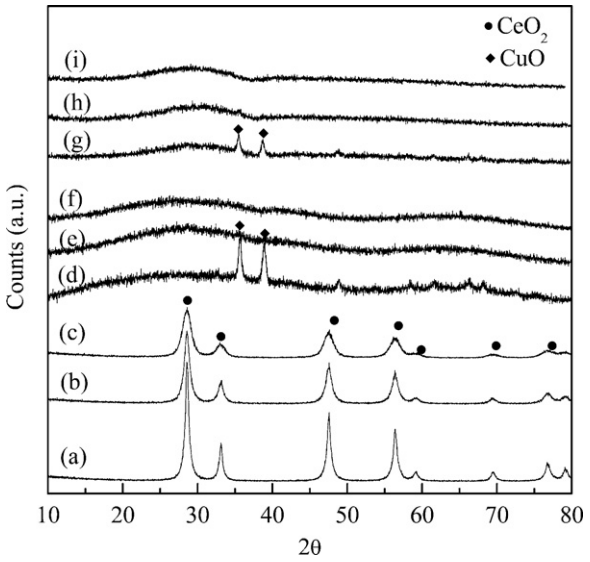

Fig. 1. X-ray diffraction (XRD) patterns of supported catalysts: (a) $5CuO/CeO_2$, (b) $2.5CuO/CeO_2$, (c) $1CuO/CeO_2$, (d) $5CuO/Al_2O_3$, (e) $2.5CuO/Al_2O_3$, (f) $1CuO/Al_2O_3$, (g) $5CuO/CeO_2–Al_2O_3$, (h) $2.5CuO/CeO_2–Al_2O_3$, (i) $1CuO/CeO_2–Al_2O_3$. Radiation: Cu-Kα (λ = 1.5406 Å, 40 kV, 30 mA); scanning velocity: $2\theta\ min^{-1}$.

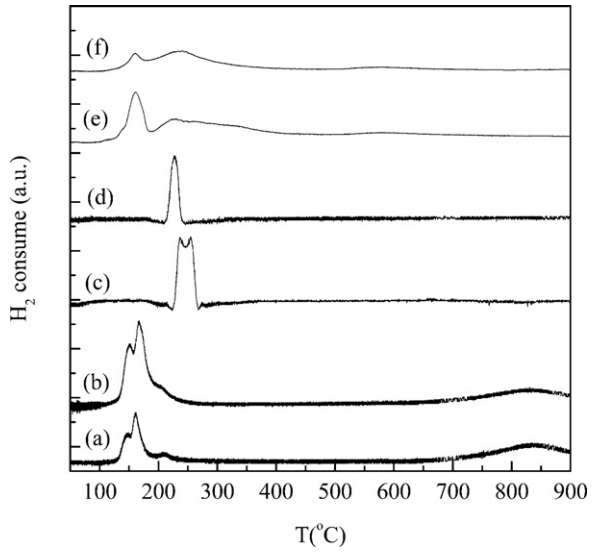

Fig. 2. Temperature-programmed reduction profiles of catalysts: (a) $5CuO/CeO_2$, (b) $2.5CuO/CeO_2$, (c) $5CuO/Al_2O_3$, (d) $2.5CuO/Al_2O_3$, (e) $5CuO/CeO_2–Al_2O_3$, (f) $2.5CuO/CeO_2–Al_2O_3$. Sample weight: 50 mg; feed composition H_2 (10%)–N_2 (90%); gas flow: 30 $cm^3\ min^{-1}$, heating rate: 10 °C min^{-1}.

Additionally, *in situ* XANES-PROX measurements were performed at the Cu K-edge. The setup was similar to that used in the H_2-TPR/XANES experiments, except that after catalyst reduction, a flow of 4%CO, 2%O_2, 50%H_2 and He was introduced into the reactor at 130 °C for 30 min.

3. Results and discussion

3.1. Characterization of catalysts

XRD patterns of the oxidized catalysts are presented in Fig. 1. In all three xCuO/CeO_2 catalysts, no CuO peak was observed, but the fluorite-like diffraction pattern of CeO_2 was detected, which suggests that either the CuO was finely dispersed on the surface of the ceria, the copper particles were smaller than the resolution limit of the technique (10 nm) or a Cu–Ce–O solid solution was formed. It might also suggest a combination of these phenomena [1,7,10–11]. The intensity of CeO_2 diffraction peaks and the average crystallite sizes of CeO_2 (determined from to the Scherrer's equation and shown in Table 1) increased with the CuO loading, which indicates solid-solid interaction, where a part of CuO diffuses into the CeO_2. On the other hand, diffraction lines due to CuO were detected only in $5CuO/Al_2O_3$ and $5CuO/CeO_2–Al_2O_3$, and this should be ascribed to heterogeneous dispersion and partial aggregation of a copper species on the surface of these solids [11]. No γ-Al_2O_3 peak appears in the Al_2O_3 and $CeO_2–Al_2O_3$ patterns, suggesting amorphous structures.

The TPR analyses performed to obtain information on the reducibility of the species and to identify the temperature at which the catalysts should be activated are presented in Fig. 2. The TPR of the solids with 1% CuO loading are not sufficiently sensitive for CuO reduction to be analyzed. According to Moretti et al., the TPR profile of CuO shows one peak at 400 °C, due to complete reduction of Cu^{2+} to Cu^0, while CeO_2 leads to a peak at 600 °C that represents a limited reduction (about 5%) of Ce^{4+} to Ce^{3+}, which can be related to a surface reaction, probably forming oxygen vacancies [16]. Ratnasamy et al. showed that CeO_2 exhibits two peaks at 385 and 521 °C, which are attributable to the reduction of surface and bulk ceria, respectively [17]. According Cheekatamarla et al., the oxygen anions attached to surface Ce^{4+} are reducible at 500 °C, while the bulk oxygen anion that is bound to Ce^{4+} in bulk ceria is reducible at 750 °C [18]. In Fig. 2, all catalysts supported on alumina showed a peak with a maximum at 294 °C, markedly lower than that of pure CuO. Moretti et al. suggested that the redox properties of CuO are significantly affected by the interaction with ceria and/or alumina, and that small CuO clusters and/or isolated Cu^{2+} ions are reduced at lower temperatures than larger CuO particles [16].

According to the literature, there are three forms of copper in the Cu–Ce–O composite oxides: (a) bulk copper in copper crystallites,

Table 1
Copper dispersion, metal surface area, average copper particle size and specific surface area (BET) of the catalysts.

Catalyst	SA ($m^2\ g^{-1}$)	D_{Cu} (%)	MSA ($m^2\ g_{Cu}^{-1}$)	AV (nm)	Ceria crystallite size (nm)[a]
$5CuO/CeO_2$	54	54	79	9	10
$2.5CuO/CeO_2$	73	61	94	7	9
$1CuO/CeO_2$	89	n.d.	n.d.	n.d.	7
$5CuO/Al_2O_3$	233	56	77	9	n.d.
$2.5CuO/Al_2O_3$	278	66	90	8	n.d.
$1CuO/Al_2O_3$	297	n.d.	n.d.	n.d.	n.d.
$5CuO/CeO\ Al_2O_3$	152	26	84	7	n.d.
$2.5CuO/CeO_2Al_2O_3$	193	56	90	8	n.d.
$1CuO/CeO_2\ Al_2O_3$	198	n.d.	n.d.	n.d.	n.d.

n.d. = not determined.
[a] Determined by Scherrer equation.

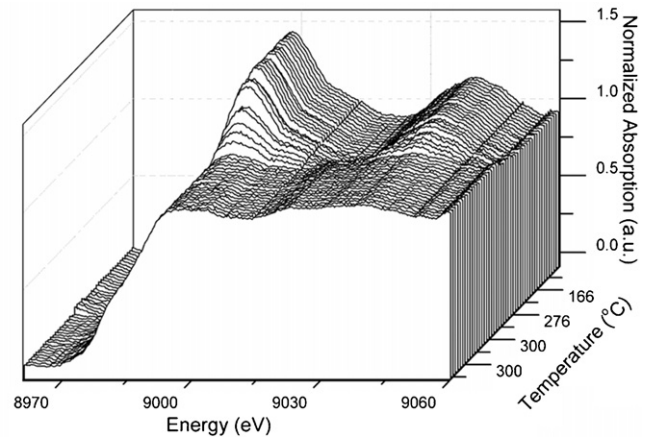

Fig. 3. In situ TPR-XANES spectra of $5CuO/CeO_2$ catalyst under reduction conditions from 25 up to 300 °C. Feed composition: H_2 (5%)–N_2 (95%); gas flow: 30 cm^3 min^{-1}, heating rate: 10 °C min^{-1} up to 300 °C.

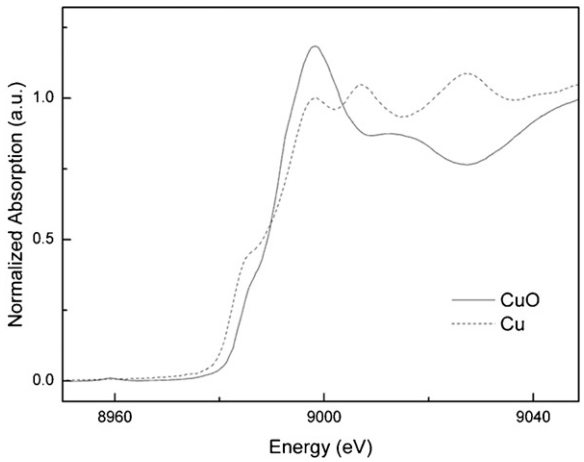

Fig. 4. Cu K-edge XANES spectra of the reference compounds.

(b) highly dispersed copper oxide, which cannot be observed by XRD and (c) bulk CuO which can be examined by XRD. It has been proposed that the third form makes little contribution to catalytic activity and that the second is the active component. There is no research that gives importance to uncombined copper and there is no report of the relationship between activity and the valence state of copper [19,20].

In Fig. 2, there are two reduction peaks for CuO supported on CeO_2, CeO_2–Al_2O_3 and Al_2O_3 and one small shoulder at approximately 200 °C for xCuO/CeO_2. The peaks at low temperature indicate the reduction of small particles of CuO which are easily reducible, and the other shows the reduction of larger particles of bulk CuO. The reduction temperature of bulk CuO is lower for xCuO/CeO_2 than for xCuO/CeO_2–Al_2O_3 and xCuO/Al_2O_3, which suggests that the CuO particles supported on CeO_2–Al_2O_3 and Al_2O_3 are larger. These observations are consistent with the XRD analyses, in which $5CuO/CeO_2$–Al_2O_3 and $5CuO/Al_2O_3$ showed diffraction peaks for CuO, indicating that these particles are sufficiently large to be detected by this technique.

The catalyst on the Al_2O_3 support with highest CuO content ($5CuO/Al_2O_3$) shows a higher copper reduction temperature due to the larger CuO particles evidenced in the XRD peaks.

Regarding the support reduction peaks, the CeO_2 is reduced at approximately 820 °C in CuO/CeO_2, this reduction being that of bulk ceria. Catalysts supported on alumina and ceria-alumina showed no reduction peaks related to the support, since alumina is not reduced at the temperature of analysis and in xCuO/CeO_2–Al_2O_3 the characteristics of alumina are more evident than those of ceria, since the ratio of CeO_2 to Al_2O_3 is 1:5.

In order to observe the changes in the oxidation state of copper species occurring during the reduction experiments, X-ray absorption spectra were recorded *in situ* from freshly calcined catalyst samples in the region near the Cu K-edge (8979 eV). Representative XANES spectra of CuO/CeO_2 are shown in Fig. 3; the results of the other catalysts were qualitatively similar and are not shown. In this case, the absorption edge energy and white line intensity are considered the main characteristics when monitoring the reduction of the copper species. In the reference samples, as shown in Fig. 4, the spectrum of CuO is characterized by a weak pre-absorption (pre-edge) peak at 8982 eV, which is attributed to the 1s–3d transition, and a sharp absorption peak at 8986 eV, due to the 1s–4p transition of Cu^{2+}, which occurs at the absorption edge and is generally called "white line". Differently, the XANES spectrum of Cu foil exhibits the edge absorption at 8979 eV, (Cu^0 1s–4p electron transition) and no "white line" [21]. Regarding the spectrum of the catalyst at room temperature shown in Fig. 3, a pre-edge feature appears at ca. 8980 eV, while the main absorption edge is observed at ca. 8983–8990 eV, which characteristics are very similar to those of the reference CuO XANES spectrum (Fig. 4). The "white line" energy value of the main edge is close to the value reported by Shimizu et al. for CuO [22]. However, as the temperature is increased under the reducing atmosphere, the white line intensity diminishes and the spectrum assumes a profile more like to that of Cu foil, implying that Cu^{2+} is being converted into Cu^0 from 140 °C. Furthermore, a shift in the absorption edge towards lower energies is observed in the course of the reaction, so that in the end it assumes a photon energy characteristic of metallic Cu.

In summary, it can be seen that, for all catalysts, the copper species are reduced in a one-step reduction process, i.e. $Cu^{2+} \rightarrow Cu^0$, without intermediate oxidation states being observed. This indicates that the various peaks observed in the TPR profiles correspond to the reduction of CuO species that interact differently with the support material.

The s-TPR data were utilized to calculate the dispersion of copper (DCu), metal surface area (MSA) and average copper particle size (AV) and these results are presented in Table 1 together with the BET surface area (SA) results.

The SA results show that catalysts with 1% CuO content had larger surface area than the others. Combining XRD, TPR and BET results, it can be suggested that this is because the small of the CuO material are smaller. This tendency can be observed in all three series of catalysts. Catalysts supported on alumina have larger SA than the others as a characteristic of the alumina support. Thus, catalysts supported on ceria have the lowest surface areas and samples of xCuO/CeO_2–Al_2O_3 have intermediate areas.

It may be noted in Table 1 that there is an increase in the values of AV with the increase of the x value in the xCuO/CeO_2 catalysts. Lee et al. [9] studied the effect of copper content on the activity of PROX-CO reaction and found that a higher content of copper favors the formation of bulk CuO with larger particles. Thus, in the $2.5CuO/CeO_2$ catalyst, the CuO showed a smaller particle size than in the $5CuO/CeO_2$ catalyst. The reaction mechanism proposed for PROX-CO with CuO/CeO_2 catalyst is the Mars–van Krevelen model [6,9,17,24]: the CO is adsorbed on the metal and oxidized by oxygen atoms of the active metal oxide, forming an oxygen vacancy and a reduced neighboring metal atom. In a second step, this reacts with O_2 and returns to the initial oxidation state. Hence, the surface metal atom is re-oxidized by oxygen gas. It is therefore important that the oxidized species are easily reduced to facilitate the redox mechanism. The sample characterization results show that these features were favored in the catalyst with lower copper content.

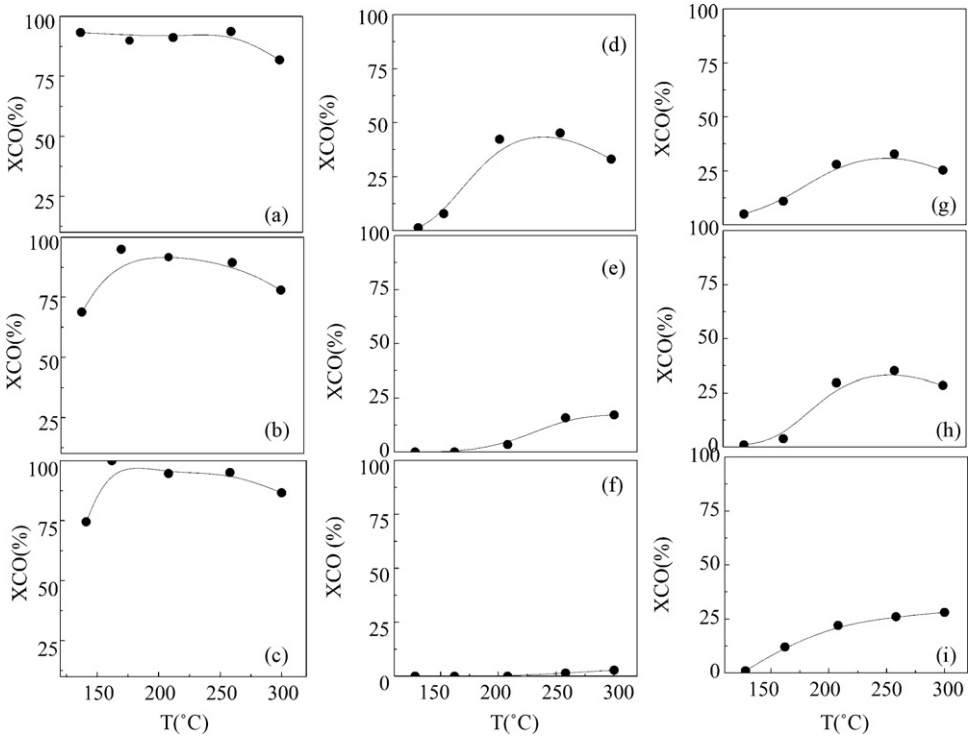

Fig. 5. Catalytic activity of (a) 5CuO/CeO_2, (b) 2.5CuO/CeO_2, (c) 1CuO/CeO_2, (d) 5CuO/Al_2O_3, (e) 2.5CuO/Al_2O_3, (f) 1CuO/Al_2O_3, (g) 5CuO/CeO_2–Al_2O_3, (h) 2.5CuO/CeO_2–Al_2O_3, (i) 1CuO/CeO_2–Al_2O_3. Feed composition: 4%CO, 2%O_2, 50%H_2 and N_2 balance; gas flow: 100 mL min^{-1}; sample weight: 400 mg.

Analysis of the s-TPR data shows that the CuO content also affects the dispersion of copper, the metal surface area and the average copper particle size. This is consistent with the H_2-TPR results, where the reduction temperature is influenced by the particle size. In 2.5CuO/CeO_2, the copper particles are more finely dispersed on the ceria surface than in the 5CuO/CeO_2 catalyst. Thus, the average copper particle size of this solid is 7 nm while it is 9 nm in 5CuO/CeO_2. The catalyst supported on Al_2O_3 or CeO_2/Al_2O_3 showed the same tendency. The above considerations are important to understand the behavior of the catalysts in the PROX-CO reaction.

3.2. Catalytic activity measurements

Figs. 5 and 6 present the catalytic activity in the preferential oxidation of CO. It can be observed that the *x*CuO/CeO_2 catalysts are more active than *x*CuO/CeO_2–Al_2O_3 and *x*CuO/Al_2O_3. Besides the beneficial effect of the strong metal–support interaction of the CuO-CeO_2 system, an important characteristic of ceria should be considered: its ability of storing and releasing oxygen on the catalyst surface. This surface oxygen could participate in the CO oxidation and enhance the activity of ceria-supported catalysts, giving the catalysts supported on ceria a higher catalytic activity. In general, the *x*CuO/CeO_2 series achieved excellent CO conversion. The 1CuO/CeO_2 catalyst should be highlighted: it is the most active of all, especially at low temperatures, with 100% conversion in the range of 150–100 °C. The beneficial effect of low temperature on the CO_2 selectivity was also observed by Ratnasamy et al. [17] and Lee et al. [19]. According to Gamarra et al. [25], at low reaction temperature, the competition for the active oxygen of the H_2 oxidation reactions is weak, favoring the high selectivity to CO_2 formation. At higher temperatures, CO and H_2 compete for active oxygen, resulting in a decline on the CO_2 selectivity, according to the redox mechanism of Mars–van Krevelen.

Zheng et al. suggested that the activity of Cu–Ce–O catalysts derived primarily from the combination of finely dispersed copper and cerium oxide and that bulk copper oxide made a negligible contribution. Thus, the dispersed CuO is responsible for the low-temperature CO oxidation. This implies that strong metal–support interaction affects the catalytic activity [10]. The amount of surface oxygen available for reduction is then controlled by the CeO_2 crystal size and dispersion of copper species [1]. Marino et al. suggested that the PROX-CO reaction takes place at the metal–support interface and the enhanced activity of the ceria-supported copper catalysts could arise from the very specific sites created at the copper nanoparticle perimeter [23].

The activity is enhanced as CuO loading increases in the tests with *x*CuO/CeO_2–Al_2O_3 and *x*CuO/Al_2O_3 catalysts. Therefore, the maximum XCO is 45% at 200 °C for 5CuO/Al_2O_3 and 40% at 250 °C for 5CuO/CeO_2–Al_2O_3 and 2.5CuO/CeO_2–Al_2O_3. At low temperatures, XCO decreases for all catalysts supported on ceria-alumina or alumina. These results suggest that the weak interaction between copper and alumina is responsible for this behavior.

The presence of larger copper particles reduces the interface area, thus weakening the metal–support interaction. The sample characterization results show that the copper supported on ceria has smaller particles and greater dispersion than on other supports. This suggests that the strong interaction between copper and ceria is responsible for the enhancement of low-temperature activity of the PROX-CO reaction on these catalysts [11].

The results for CO_2 selectivity are shown in Fig. 6. They are similar to those for XCO: the CuO/CeO_2 catalysts are the most selective, especially at low temperatures and a tendency for SCO_2 to fall with increasing temperature can be observed. Catalysts supported on alumina or ceria-alumina exhibited a selectivity enhance with an increase in temperature. In other words, the temperature accelerates the $H_2 + O_2$ reaction due to its less exothermic nature. Thus, the decrease in selectivity with rising temperature was clearly related to this reaction. Methane formation was not observed under these experimental conditions.

The oxidation profile of the CuO/CeO_2 catalyst in the presence of reactants was also investigated by XANES analysis. In this case, the CuO/CeO_2 catalyst was chosen as a representative example.

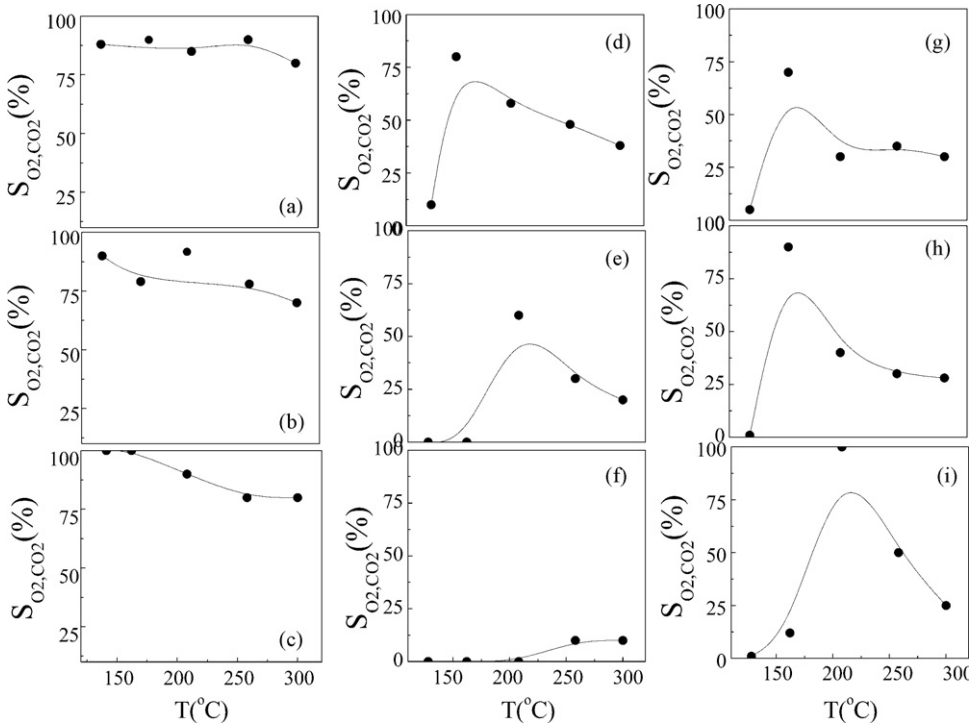

Fig. 6. Selectivity to CO_2. (a) $5CuO/CeO_2$, (b) $2.5CuO/CeO_2$, (c) $1CuO/CeO_2$, (d) $5CuO/Al_2O_3$, (e) $2.5CuO/Al_2O_3$, (f) $1CuO/Al_2O_3$, (g) $5CuO/CeO_2–Al_2O_3$, (h) $2.5CuO/CeO_2–Al_2O_3$, (i) $1CuO/CeO_2–Al_2O_3$. Feed composition under 4%CO, 2%O_2, 50%H_2 and N_2 balance; gas flow: 100 mL min^{-1}; sample weight: 400 mg.

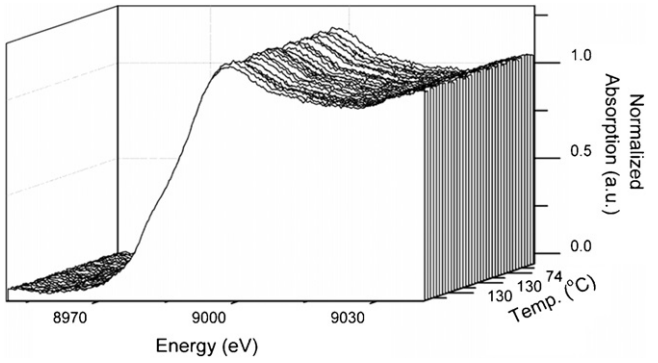

Fig. 7. *In situ* PROX-CO-XANES spectra for the CuO/CeO_2 catalyst.

Fig. 7 shows that the oxidation profile of the catalyst remained unchanged between 74 and 130 °C, and no re-oxidation of the reduced copper species occurred under the reaction conditions, since all XANES spectra were similar to that of Cu^0.

4. Conclusions

The combination of preparation method and calcination conditions resulted in active and selective solids for PROX-CO, especially for the ceria-supported catalysts. The copper loading is an important parameter for catalytic performance. The $1CuO/CeO_2$ sample was the most active and selective, particularly at low temperatures as 100 °C, suitable for PEMFC applications. It was observed by characterization techniques that the presence of small particles of Cu interacting with ceria is crucial. This catalyst had the largest metallic area, the smallest particle size, the highest dispersion of copper species and the strongest metal–support interaction. On the other hand, the CuO/Al_2O_3 catalysts, despite the higher BET surface area, showed the largest particles and were the hardest to reduce. Thus, the metal–support interaction explains the differences between ceria and alumina supports. In the ceria-supported catalysts other characteristics were relevant, such as the surface area and metal dispersion; the redox properties of the ceria support also contributed to catalytic performance. Raising the temperature resulted in a catalytic activity and the best results were found at 100 °C for ceria-supported catalysts. The catalysts supported on alumina showed a contrary tendency to this behavior.

Acknowledgement

The authors are grateful to Capes, CNPq and FAPESP for the financial support.

References

[1] A. Gómez-Córtes, Y. Márquez, J. Arenas-Alatorre, G. Diaz, Catal. Today 133–135 (2008) 743.
[2] Z. Liu, R. Zhou, X. Zheng, J. Nat. Gas Chem. 17 (2008) 125.
[3] Y. Zhang, H. Liang, X.Y. Gao, Y. Liu, Catal. Commun. 10 (2009) 1432.
[4] G. Avgouropoulos, J. Papavasiliou, T. Tabakova, V. Idakiev, T. Ioannides, Chem. Eng. J. 124 (2006) 41.
[5] A. Martinez-Arias, D. Gamarra, M. Fernandez-Garcia, A. Hornes, P. Bera, Z. Koppany, Z. Schay, Catal. Today 143 (2009) 211.
[6] G. Sedmack, S. Hocevar, J. Levec, J. Catal. 213 (2003) 135.
[7] J.W. Park, J.H. Jeong, W.L. Yoon, C.S. Kim, D.K. Lee, Y. Park, Y.W. Rhee, Int. J. Hydrogen Energy 30 (2005) 209.
[8] L. Chung, C. Yeh, Catal. Commun. 9 (2008) 670.
[9] H.C. Lee, D.H. Kim, Catal. Today 132 (2008) 109.
[10] X. Zheng, X. Zhang, X. Wang, S. Wang, S. Wu, Appl. Catal. A: Gen. 295 (2005) 142.
[11] X. Tang, B. Zhang, Y. Li, Y. Xu, Q. Xin, W. Xhen, Catal. Today 93 (2004) 191.
[12] K. Zhou, R. Xu, X. Sun, H. Chen, Q. Tian, D. Shen, Y. Li, Catal. Lett. 3 (2005) 169.
[13] C.S. Polster, H. Nair, C.D. Baertsch, J. Catal. 266 (2009) 308.
[14] M. Manzoli, R.D. Monte, F. Boccuzzi, S. Coluccia, J. Kaspar, Appl. Catal. B: Environ. 61 (2005) 192.
[15] A. Gervasini, S. Bennici, Appl. Catal. A: Gen. 281 (2005) 199.
[16] E. Moretti, M. Lenarda, L. Storaro, A. Talon, T. Montanari, G. Busca, E. Rodríguez-Castellón, A. Jiménez-López, M. Turco, G. Bagnasco, R. Frattini, Appl. Catal. A: Gen. 335 (2008) 46.
[17] P. Ratnasamy, C. Srinivas, C.V.V. Satyanarayana, P. Manikandan, R.S.S.S. Kumaran, M. Sachin, V.N. Shetti, J. Catal. 221 (2004) 455.
[18] P.K. Cheekatamarla, W.S. Epling, A.M. Lane, J. Power Sources 147 (2005) 178.

[19] Z. Shanghong, B. Xue, W. Xiaoyan, Y. Wenguo, L. Yuan, J. Rare Earths 24 (2006) 177.
[20] L. Chung, C. Yeh, Catal. Comunn. 9 (2008) 670.
[21] S. Velu, K. Suzuki, C.S. Gopinath, H. Yoshida, T. Hattori, Phys. Chem. Chem. Phys. 4 (2002) 1990.
[22] K. Shimizu, H. Maeshima, H. Yoshida, A. Satsuma, T. Hattori, Phys. Chem. Chem. Phys. 2 (2000) 2435.
[23] F. Mariño, C. Descorme, D. Duprez, Appl. Catal. B: Environ. 58 (2005) 175.
[24] X. Donga, H. Zou, W. Lin, Int. J. Hydrogen Energy 31 (2006) 2337.
[25] D. Gamarra, G. Munuera, A.B. Hungría, M. Fernández-García, J.C. Conesa, P.A. Midgley, X.Q. Wang, J.C. Hanson, J.A. Rodríguez, A. Martínez-Arias, J. Phys. Chem. C 111 (2007) 11026.